Effect of iPP molecular weight on its confinement within mesoporous SBA-15 silica in extruded iPP–SBA-15 nanocomposites

Rosa Barranco-García[1], José M. Gómez-Elvira[1], Jorge A. Ressia[2,3], Lidia Quinzani[2], Enrique M. Vallés[2], Ernesto Pérez[1], María L. Cerrada[1*]

[1]Instituto de Ciencia y Tecnología de Polímeros (ICTP-CSIC), Juan de la Cierva 3, 28006 Madrid, Spain.

[2]PLAPIQUI (UNS-CONICET), Camino La Carrindanga km 7, 8000 Bahía Blanca, Argentina

[3]Comisión de Investigaciones Científicas de la Provincia de Buenos Aires (CIC), 1900 La Plata, Argentina

Correspondence to: mlcerrada@ictp.csic.es

Abstract

Different nanocomposites based on two isotactic polypropylenes (iPP) and mesoporous SBA-15 silica have been attained by melt extrusion as an attempt to understand the influence of average molecular weight in the rheological behavior, morphological and crystalline features and in the final properties (thermal stability and mechanical response) as well as in the capability of incorporating iPP chains within the nanometric SBA-15 pores. Closeness to rheological percolation and a significant increase of viscosity are observed as SBA-15 content is raised, this effect being more evident for the materials prepared from the iPP with the lowest molecular weight. These composites also shift their maximum degradation to lower values under inert atmosphere but keep rather unchanged decomposition behavior in oxidant conditions. No considerable changes are found with molecular weight in their morphological characteristics, nor in the type of iPP polymorph developed. The confinement of iPP chains in the SBA-15 channels, implied by a small endotherm in the DSC melting curves, is definitely ascertained by real-time variable-temperature Small Angle X-ray Scattering measurements with synchrotron radiation, suggesting, additionally, that somewhat thicker crystallites are developed within the mesostructure in the materials prepared from the iPP with inferior molecular weight. Moreover, the SBA-15 mesoporous particles exert a reinforcing role in all cases and reduce the deformation capacity of the ultimate materials as their content is increased.

Keywords: iPP/SBA-15 nanocomposites; rheological percolation; synchrotron SAXS measurements; reinforcement; molecular weight.

1. Introduction

Isotactic polypropylene (iPP) is used widely in industry and daily life because it is a thermoplastic that shows a good performance in processing and practical applications as well as a low price. Thus, iPP is the second most abundantly produced plastic worldwide and more than 50 million metric tons of iPP are manufactured annually [1]. At practical level, iPP is often filled with organic or inorganic particles to enhance mechanical response and reduce costs [2-6]. For instance, iPP can be filled with metallic powders to provide functionality [7-11]. Moreover, pristine and modified silicas have been frequently added to iPP to boost other specific characteristics [12-16] that allow spreading out its application fields.

Ordered mesoporous silicas are a specific and relatively new type, which were firstly described in literature [17] in 1992. The MCM-41 is the best-known member. Years later, a new family was also synthesized [18,19] at Santa Barbara University and the SBA-15 became the most used constituent of this series. These mesoporous silicas are characterized by presence of well-organized arrangements, which are hexagonal frames in both the MCM-41 and the SBA-15. Main difference between them is their pore size, whose diameter ranges from 2 to 4 nm and from 5 to 20 nm, respectively. These ordered hollow silicas on the nanoscale have found diverse applications in distinct sectors, among others: catalysis, coatings, optics, drug delivery, diagnostics, gas-separation, bio-separation, cosmetics, and nanotechnology. Existence of these mesostructures, which are constituted by ordered long channels, becomes a very attractive characteristic for their use as a minor component in polymeric based materials. Together with a reinforcement effect, these (nano)particles can act also either as confinement spaces or as pores depending on if polymeric chains are or not capable, respectively, to fully take up their nanometric channels. As example of the former, the mesoporous silicas acted as a nanoreactor during in situ polymerization and PE nanofibers reported by Dong et al. [20] when fixing Cp_2ZrCl_2 on MCM-41 and SBA-15. In other investigation by Xu et al. [21], polyethylene with fibrous morphology was attained on SBA-15 supporting an iron(II)-bisimine pyridine catalyst, the polymer showing higher molar

mass than its homogeneous counterpart. PE nanofibers were also described by Campos et al. [22,23] when a zirconocene supported on MCM-41 and Al containing MCM-41 carriers were used. On the other hand, mixed matrix membranes might be produced if mesoporous silica behaves as porous material. Then, large increases in gas permeability should be observed mainly if surface of mesoporous silica is functionalized, avoiding agglomeration of silica particles [24-27].

A precise knowledge of existence of an eventual confinement effect is a mandatory aspect to be resolved in the polymeric materials incorporating these mesoporous silicas. Differential Scanning Calorimetry (DSC) turned out very useful in nanocomposites based on high density polyethylene (HDPE) with either pristine or decorated MCM-41 particles attained by in situ polymerization [28-30] owing to the appearance of a secondary melting process ranging from 65 to 85 °C. This less intense endothermic event is shifted to higher temperatures, in the 100-115 °C range, if SBA-15 is used [31-33] instead of MCM-41 during polyethylene polymerization. Accordingly, pore size of the mesostructured silica seems to be the key parameter. This low-temperature endotherm has been also found more recently in materials based on iPP and SBA-15 [34].

Real-time variable-temperature small-angle X-ray scattering (SAXS) measurements with synchrotron radiation have been proved as a powerful tool to demonstrate presence of iPP chains within SBA-15 channels in nanocomposites prepared by melt extrusion [35]. The results showed a discontinuity at temperatures ranging from 95 to 120 °C in the intensity of the (100) diffraction of the hexagonal arrangement of SBA-15. Its magnitude was strongly dependent on SBA-15 content and variation in the area of this diffraction was attributed to the change in the scattering contrast before and after the melting of the ordered iPP chains confined inside the SBA-15 pores.

The main objective of the present investigation is to go a step further and learn the influence that iPP molecular weight has on polymer confinement inside the SBA-15 channels. Additionally, the effect on the rheological characteristics, on the morphological and crystalline features and on the final properties (as thermal stability or mechanical behavior) of the resultant materials is also analyzed. Thus,

numerous techniques have been employed in this research, including: size exclusion chromatography (SEC), scanning electron microscopy (SEM), wide and small angle X-ray experiments (WAXD and SAXS, respectively) with synchrotron radiation, differential scanning calorimetry (DSC), thermogravimetry (TGA), rheological experiments in the molten state, and stress-strain (σ-ε) tests in solid films.

2. Experimental part

2.1. Materials and chemicals

Two commercially available metallocene-catalyzed isotactic polypropylenes (Metocene X50081: melt flow index of 60 g/10 min, and Metocene HM562P: melt flow index of 15 g/10 min at 230 °C/2.16 kg, ASTM D1238, both kindly supplied by LyondellBasell) have been used in the present research as polymeric matrices. The SBA-15 particles were purchased from Sigma-Aldrich (specific surface area, S_{BET}= 517 m^2/g; total pore volume, V_t = 0.83 cm^3/g; average mesopore diameter [36], D_p= 6.25 nm) and were used as received.

2.2. (Nano)composite and film preparation

Composites with different contents in SBA-15 particles (0, 2, 4, 7, 12 % in weight for the iPP with the lowest average molecular weight, named as iPPL, iPPSBA2L, iPPSBA4L, iPPSBA7L and iPPSBA12L; and, 0, 1, 4, 8 and 13 % in weight for the iPP with the highest average molecular weight, being labeled as iPPH, iPPSBA1H, iPPSBA4H, iPPSBA8H and iPPSBA13H, respectively) were processed by melt extrusion in a corotating twin-screw microextruder (Rondol). Both polymer and SBA-15 were dried previously for 24 h under vacuum at 110 °C. A screw temperature profile of 190, 185, 180, 170 y 115 °C was used from the die to the hopper, being the length-to-diameter ratio 20:1. Then, films were obtained by compression molding at 190 °C and at 30 bar for 6 minutes in a hot-plate Collin press (model 200x200). A relatively fast cooling process (rate around 80 °C/min) was applied between plates under pressure (30 bar) to the different films from their melt to room temperature.

2.3. Sample Characterization and Properties

The molecular weights and molecular weight distributions for the two isotactic polypropylenes used as polymeric matrices in this investigation were determined by Size Exclusion Chromatography (SEC) using a Waters 150-C ALP/GPC equipped with a set of three PL-GEL MIXED-A columns from Polymer Labs. The solvent used was 1, 2, 4-trichlorobenzene (TCB) at 135 °C with 1 mL/min flow. The apparent molecular weights of the polymers were estimated following the standard calibration procedure using monodisperse polystyrene samples and the corresponding Mark-Howink coefficients for linear polypropylene [37]. The M_w values obtained for the extruded polymers were 135,000 and 173,000 g/mol for iPPL and iPPH, respectively. Their polydispersity was 1.9 and 2.0, respectively.

Rheological characterization was carried out in small-amplitude oscillatory shear mode using a dynamic rotational rheometer TA Instruments ARG2 (New Castle, USA). The tests were performed under nitrogen atmosphere using parallel plates of 25 mm in diameter, at a frequency range between 0.1 and 100 rad/s, and a temperature interval of 180-220 °C. All tests were carried out at small stresses in order to assure the linearity of the dynamic responses [38].

Scanning electron microscopy, SEM, observations were carried out at room temperature for some of the studied materials in a LEO EVO-40 XVP equipment operated at 15 kV. The sliced sections were obtained by cutting at -70 °C with a Leica UCT EM-FCS ultra-microtome equipped with a diamond knife. Prior observation, these sections were chemically etched in order to enhance contrast between the iPP polymer and the mesoporous particles. This etching treatment consisted of the immersion of samples in a solution of 0.2 % v/v potassium permanganate in sulfuric acid for 6 min. Subsequently, they were washed several times with distilled water and 20% v/v hydrogen peroxide.

Calorimetric analyses were carried out in a TA Instruments Q100 calorimeter connected to a cooling system and calibrated with different standards. The sample weights were around 3 mg. A temperature interval from -40 to 180 °C was studied at a heating rate of 20 °C/min. For the

determination of the crystallinity, a value of 160 J/g was used as the enthalpy of fusion of a perfectly crystalline material [39-41].

Real-time variable-temperature simultaneous SAXS/WAXD experiments were carried out with synchrotron radiation in beamline BL11-NCD at ALBA (Cerdanyola del Valles, Barcelona, Spain) at a fixed wavelength of 0.1 nm. An ADSC detector has been used for SAXS (off beam, at a distance of 294 cm from sample) and a Rayonix one for WAXD (at about 19 cm from sample, and a tilt angle of around 30 degrees). A Linkam Unit, connected to a cooling system of liquid nitrogen, was employed for the temperature control. The calibration of spacings was obtained by means of silver behenate and Cr_2O_3 standards. The initial 2D X-ray images were converted into 1D diffractograms, as function of the inverse scattering vector, $s = 1/d = 2 \sin \theta/\lambda$. Film samples of around 5×5×0.1 mm were used in the synchrotron analysis.

Thermogravimetric analysis (TGA) was performed in a Q500 equipment of TA Instruments under air or nitrogen atmosphere at a heating rate of 10 °C/min. Determination of the SBA-15 amount in the nanocomposites prepared by extrusion has been carried out as an average of the values obtained under the two atmospheres. The resulting values of the SBA-15 content are listed in Table 1.

Nominal stress-strain tests were performed at a temperature of 25 °C and a stretching rate of 10 mm/min in a MTS Q-Test Elite dynamometer with a load-cell of 100 N. Specimens for these experiments were punched out from the polymer films. The dimensions of these strips were 15 mm long, 1.9 mm wide and around 0.10 mm thick. At least, six different strips were stretched until fracture for a given specimen.

3. Results and discussion

The viscoelastic behavior in the molten state of iPP–SBA-15 (nano)composites prepared by extrusion has been investigated to evaluate the effect of iPP molecular weight on composites containing equivalent amounts of SBA-15. Figure 1 displays the results for the storage (G') shear modulus as well as for viscosity (η') of these (nano)composites. It is well known that bi-logarithmic plots of the isotherms

of the $G'(\omega)$ and $G''(\omega)$ can be superimposed in thermo-rheologically simple materials by horizontal shifts log (a_T) along the frequency axis, log (ω), and vertical shifts given by log (b_T), such that [38,42]: b_T G' (a_T ω, T) = G' (ω, T_{ref}), being T_{ref} the reference temperature, and b_T G'' (a_T ω, T) = G''(ω, T_{ref}). For the dynamic viscosity, relationship to be accomplished is: (b_T/a_T) η' ($a_T\omega$, T) = η' (ω, T_{ref}).

Figure 1 and Table 1 clearly show that independently of the frequency G′, G″ and η′ parameters in the iPP with higher M_w (iPPH) and in their respective composites are larger than the values exhibited by the iPPL and materials prepared from it, at similar SBA-15 content. This feature is related to variation of entanglements capability and their relaxation times, both increasing as molecular weight rises [38]. In spite of difference in molecular weights is not too large (135,000 and 173,000 g/mol for iPPL and iPPH, respectively), variations in the rheological response are quite noticeable, pointing out the importance of chains dynamics.

Moreover, these magnitudes become higher as growing amount of mesoporous silica is added. This fact is more evident at the highest SBA-15 contents. All isotherms measured for the two neat iPPs and for the various iPP–SBA-15 (nano)composites can be superimposed, independently of the molecular weight of the iPP matrix. The only exceptions are the materials that incorporate the highest amount of SBA-15. These two composites, iPPSBA12L and iPPSBA13H, exhibit a thermo-rheological complex behavior, contrary to that found in the two iPP homopolymers and the rest of SBA-15 based materials where specimens show the common terminal flow law. Thus, G″ values at 200 °C are higher than the G′ ones (see values listed in Table 1) and power-law dependences are close to ω^2 and ω [38], for G′ (depicted in Figure 1 (a) and (b)) and G″ (not shown).

Storage and loss moduli dependences with frequency become, however, altered in the iPPSBA12L and iPPSBA13H. Accordingly, slopes decrease. Differences between G″ and G′ are then reduced (see values in Table 1) and the elastic component starts to be predominant at those very low frequencies, indicating the closeness of a transition from a liquid to a solid-like behavior. This change has been explained by formation of a temporary network due to percolation of fractal filler aggregates

interconnected by bridging polymer chains [43-44]. It has been named as rheological percolation. At longer time scales, i.e., much smaller frequencies, this network could finally be relaxed by different mechanisms as the adsorbed polymeric molecules are released [11]. Similar response has been described [45] whereas other distinct ones have been also reported in iPP based composites [46]. Changes in behavior can be related to differences in particle shape, size, state of dispersion and concentration. Each system is particular and there are not previous results related to iPP–SBA-15 materials. It is known that aspect ratio of the filler has a very important role and rheological percolation threshold is promoted as aspect ratio increases.

Viscosity variation is also sensitive to this phenomenon. Consequently, the iPPs and the composites up to around 8 wt.% in SBA-15 display a Newtonian response of viscosity on frequency, being the values for the iPP with high M_w and its compounds significantly higher than those obtained from iPPL. This viscosity independence at low frequency values is no longer observed in iPPSBA12L and in iPPSBA13H materials. Moreover, closeness of the rheological percolation threshold affects more importantly to iPPSBA12L and iPPSBA13H, as deduced from lower plots of Figure 1. Those results show that SBA-15 influence is stronger in the molten state of an iPP with lower molecular weight.

Figure 2 depicts the variation with frequency, at 200 °C, of the phase angle δ, showing a change in the reinforcement effect triggered by SBA-15, which is dependent on the iPP molecular weight. Thus, the values of the phase angle at high frequencies for the homopolymer with the highest M_w and its composites at mesoporous silica contents up to around 8 wt.% are lower than those corresponding to iPP with inferior molecular weight. This feature indicates that viscous component of the former at that temperature contributes to the total value of G* in a smaller extent than in the iPP with the low molecular weight and its materials. As frequencies are reduced, phase angle tends to 90 °.

The exceptions are again the two composites with highest SBA-15 contents. Thus, iPPSBA13H sample shows a value about 70 ° at low frequency because liquid to solid-like transition is approaching at that SBA-15 amount. Behavior exhibited by iPPSBA12L is even rather different. Phase angle goes

through a maximum with frequency and the δ values at low frequency range are much smaller in iPPSBA12L than in iPPSBA13H, pointing out that elastic component affects relatively more due to the difference in molecular weights. Thus, the reinforcement effect of mesoporous silica in the molten matrix seems to be more important at high SBA-15 contents as molecular weight decreases. In fact, liquid to solid-like transition at low frequencies is more noticeable in iPPSBA12L than in iPPSBA13H.

Presence of mesoporous silica does not only affect iPP rheological characteristics, as just shown, but might influence its thermal stability in the molten state. In fact, the efficiency of MCM-41 mesoporous silica has been reported [47-49] in literature as promoter towards degradation of polyolefins into liquid fuels. In the present case, Figure 3 shows the TGA curves under inert and oxidative conditions, respectively, for all the different materials analyzed. Besides information about polymer degradation, the weight remaining at high temperatures allow determining the SBA-15 wt. % content in the composites. The results for the two measurements and the average value are presented in Table 2.

As expected, decomposition process under an inert environment is simpler than in presence of oxygen, independently of iPP molecular weight and SBA-15 incorporation. Thus, it takes place through a single stage from 350 to 550 °C. The reaction products of polypropylene pyrolysis have been described to consist of four major categories: alkanes, alkenes, dienes, and aromatic compounds [50].

Several degradation processes are, however, observed from 200 to 550 °C under air, as clearly noticed from the DTGA curves in Figure 4. Formation of alkyl radicals from polymeric chains is reported to be the first stage in polyolefins thermal oxidation, followed by reaction with the oxygen of alkyl radicals to produce hydroperoxides [51-52], which can decompose to alkoxyl radicals. Then, hydrogen from the chain and other alkyl radicals are abstracted by alkoxyl radicals. Finally, various carbonyl species are generated.

As deduced from the corresponding inset of Figure 3 and from Figure 4a, degradation under nitrogen initiates in the iPPH at temperatures lower than in iPPL, although both exhibit identical maximum degradation temperature. Incorporation of SBA-15 leads to a slight increase in thermal

stability, which is dependent on silica content in a minor extent. This effect is less important in the materials prepared from iPPL with the lowest molecular weight, as noted in Figures 3, 4a and 4c.

The trend is different if experiments are performed under air. Decomposition processes occur in a broad temperature interval for all the samples. Temperature of the maximum degradation is around 7°C higher in iPPL than in iPPH. Addition of SBA-15 particles significantly contributes to thermally stabilize the resultant materials. At low contents, this effect is more evident in those prepared from iPPH while differences related to iPP molecular weight become smaller for the highest silica contents. Moreover, shape of decomposition curves changes at those high mesoporous amounts independently of iPP M_w. Two maxima appear in the derivative curves: a very broad one is observed at low temperature together with a much narrower process at higher temperatures, as noticed in Figure 4.
The effective delay observed in the build-up of the distinctive degraded species under both conditions has been associated [53] with the increase in viscosity of the molten material, larger as SBA-15 content is raised. The iPP chain dynamics is gradually constrained and the temperature at which anaerobic chain scission occurs rises. Under oxidative conditions, a hindrance of the diffusion of air into the bulk is supposed and, thus, a delay in the oxidation of iPP chains takes place.

Which are the features of these materials in the solid state when are processed as films? Is there any effect of iPP molecular weight in their behavior, as that observed in the rheological response? To answer these questions, a complete evaluation of morphological details and crystalline characteristics is mandatory.

Figure 5 shows the SEM micrographs found in the composites prepared from these two iPPs at the two highest SBA-15 contents. Size and shape of the silica particles have been reported to be around 350 nm wide and 0.9 μm long, exhibiting a characteristic vermicular elongated shape [34]. It can be deduced from Figure 5 that SBA-15 silica is rather uniform and randomly distributed in the two PP matrices. Accordingly, a minor agglomeration of particles takes place, as deduced from these micrographs.

Extrusion processing and the further film preparation by compression leaded to a suitable and homogeneous SBA-15 dispersion with absence of a significant aggregation within the polypropylene matrix. Thus, silica is completely embedded within the matrix without existence of inorganic domains of large size across the surface, independently of iPP molecular weight. These characteristics seem to indicate a good adhesion at the filler–matrix interface and an intimate contact between the SBA-15 and polypropylene. In addition, rheological results are corroborated and the closeness of quite individual particles is observed as SBA-15 content increases, explaining the occurrence of common features in rheological percolation threshold.

Figure 6 show DSC curves for the different materials under analysis during first melting process (upper representations) and further cooling from the melt (lower representations), both performed at a rate of 20°C/min. The top plots noticeably display two clear endothermic events: the one appearing at high temperature, at around 140 °C, which involves the larger amount of enthalpy; and another endotherm, with much less intensity, that occurs at the interval of about 95-115 °C. The former is associated with the melting of regular polypropylene chains while the latest is related to crystallites that are supposedly thinner and with much smaller sizes, which correspond, most probably, to the ones developed within the nanometric SBA-15 channels.

DSC experiments have proved the existence of confined crystallites inside porous materials for organic solvents in controlled pore glasses [54] and for semicrystalline polyolefins within mesoporous silica [28-35], as commented in Introduction, through the appearance of an endotherm that shows a depression of melting point (and a reduced enthalpy). The sensitivity of this technique does not allow observing the process at the lowest SBA-15 contents, being necessary a minimum amount of iPP crystals within the mesostructure to be detectable. This is ranging from 4 to 7 wt.% in the present materials. A displacement of this minor melting process to high temperatures is observed for the nanocomposites prepared from the iPP with the lowest molecular weight as main effect of different M_w evaluated, as seen in Figure 6 a) and b). Thus, the melting temperature (T_m) for this small process is

around 104 °C in iPPSBA8H and iPPSBA13H compared with the 109 °C found in iPPSBA7L and iPPSBA12L. On the other hand, there are not differences in the enthalpy involved. These features seem to indicate that crystals developed in the interior of the SBA-15 channels are thicker in the nanocomposites prepared from the iPP with the lowest molecular weight. Nevertheless, rather constant T_m values are attained for the major endothermic process in all the different samples (see values in Table 2), independently of presence of SBA-15, its content and iPP molecular weight. A slightly higher crystallinity is, however, found in the iPPL and its nanocomposites.

Crystallization process is also affected by the iPP molecular weight. The shorter polypropylenic macrochains existing in iPPL are able to initiate their ordering at temperatures higher than those present in iPPH. Accordingly, T_c^{iPPL} is located at 117.5 °C while T_c^{iPPH} is 114 °C, as listed in Table 2. Incorporation of SBA-15 particles significantly delays the iPP crystallization in all the nanocomposites independently of the iPP M_w but the effect of increasing silica content is much more interesting, comparing the materials prepared from iPPL or iPPH. Thus, an important crystallization hindrance is observed in all composites, the effect being significantly higher in iPPL (peak crystallization temperatures in the composites around 7 °C lower than in the neat polymer) while that difference is only around 4 °C for composites of iPPH. And as a result, there is a coincidence of the crystallization temperatures of the two kinds of composites: all around 111 °C. A closer inspection reveals that this anti-nucleant effect seems to get slightly reduced as SBA-15 content increases for iPPL composites, while it increases slightly for iPPH ones. This behavior is different to that observed in nanocomposites synthesized by *in situ* polymerization [34] where a nucleating effect was reported at the same interval in SBA-15 content. Crystallization hindrance was observed only for SBA-15 amounts greater than 20 wt.%. It should be commented that iPP molecular weight in the resulting *in situ* nanocomposites was inferior to that for iPPL due to the catalyst used in polymerization.

The next question to be answered should be: which crystalline lattice is developed in these nanocomposites? A very interesting polymorphic behavior is exhibited by polypropylene since different

crystal lattices (α, β, γ, δ and a mesomorphic form) can be generated by changing temperature / pressure / cooling rate imposed along processing together with the incorporation of specific nucleating additives and the variation of microstructural features through synthetic conditions [55-67].

Figure 7 shows the X ray profiles at room temperature, obtained with synchrotron radiation, for the different nanocomposites. It can be observed that the monoclinic lattice is the only one formed under the present crystallization conditions [68] in these metallocene iPP matrices, independently of their M_w. Accordingly, the five main reflections, corresponding to the (110), (040), (130), (111), and (-131, 041) diffraction planes characteristic of this α crystalline modification are seen. Presence of SBA-15 particles does not influence the type of lattice developed. In spite of the metallocene origin of these two iPPs, there is not indication of presence of the orthorhombic phase because of the high cooling rate imposed through the film processing by compression.

WAXD crystallinity, f_c^{WAXD}, of the iPP polymeric component can be assessed from these profiles. As first stage, subtraction of contribution from the amorphous SBA-15 has to be carried out. Mesoporous silica particles are a completely amorphous material and its halo overlapped in this range with the iPP profile [35]. After that, the amorphous polymeric component has to be also removed. This is easily obtained from the diffractograms of the melt attained by variable-temperature WAXD (results not shown) with an appropriate shifting to account for the thermal expansion [41]. After those two subtractions, the total crystallinity values attained are detailed in Table 1. It is clearly deduced that crystallinity remains rather constant at a given iPP molecular weight after incorporation of SBA-15, this value being practically inside the experimental error (± 0.02) for all the composites. These results corroborate those found from DSC.

Real-time variable temperature SAXS profiles for the pristine SBA-15 and the composite iPPSBA1H are depicted in Figure 8. It is clearly noted the hexagonal arrangement of this mesoporous silica, which remains unchanged along the whole temperature interval analyzed. This ordering shows the reflections (100), (110), (200), (210) and (300). It is kept in iPPSBA1H (and in the rest of the

composites, independently of the iPP M_w) although its intensity is considerably lower because the content in SBA-15 particles is very small. In fact, the (210) and (300) diffractions are not seen in iPPSBA1H due to the reduced amount of SBA-15. Intensity reduction was reported for composites based on polyethylenimine (PEI) and SBA-15 [69], this lowering being increased with rising PEI content.

A wide peak is also noticeable for iPPSBA1H in the region of lower *s* values together with these diffractions ascribed to SBA-15. Its location is shifted to larger spacings leading to its complete separation from the main hexagonal SBA-15 reflection and its intensity is significantly increased prior melting. It is associated with the change in the electron density existing in the iPP matrix due to its semicrystalline nature and its lamellar crystals, *i.e.*, ascribed to its most probable long spacing. Their variations with temperature are due to the progressive iPP crystallite thickening from room temperature up to their melting, moment at which disappears because of the existence of a unique isotropic amorphous iPP state. As commented from DSC results, there are not important alterations in the T_m of those crystals developed outside of the SBA-15 channels. Consequently, analogous long spacing values are obtained in the distinct materials independently of the iPP molecular weight. A deeper analysis within this *s* interval could not turn out accurate and definite, mainly at room temperature, because of the strong overlapping between iPP long spacing and the first SBA-15 order of its hexagonal arrangement.

Real-time variable-temperature small-angle X-ray scattering (SAXS) measurements with synchrotron radiation have been recently ascertained as an effective tool to demonstrate presence of polypropylene chains within SBA-15 channels in nanocomposites prepared by melt extrusion and *in situ* polymerization [34,35,70] from the thorough analysis in the *s* range from 0.095 to 0.13 nm^{-1}, where the first order of the hexagonal arrangement of the SBA-15 particles is observed. The SAXS profiles, at that interval, during the first melting process for the different nanocomposites prepared from iPPL are shown in Figure 9a. It is observed that the position and width of its (100) reflection are unchanged with temperature from 20 °C to 180 °C, interval which includes the iPP melting. On the contrary, the different

iPPL composites represented in Figure 9a show noticeable changes in the intensity of the (100) SBA-15 diffraction. The magnitude of the observed discontinuities is dependent on SBA-15 content, but occurs at temperatures between 100 and 125 °C for all of them, being noted even for the low silica contents. This temperature interval perfectly agrees with that deduced from DSC experiments for the less intense endotherm (see inset in Figure 6a) above commented. It was tentatively associated with melting of those thin crystals confined in the nanospace of SBA-15 channels. The existence of the discontinuity in the SAXS intensity indicates that this reflection related to the first order of the hexagonal SBA-15 arrangement undergoes a change when the melting of iPP crystallites takes place in the interior of its pores. Electronic density of those confined iPP macrochains varies during this phase transition and, consequently, the scattering contrast between the walls and the inside of the SBA-15 channels is modified, allowing detection of constrained iPP crystals.

Figure 9b displays the variation in area of the (100) SBA-15 diffraction for the neat silica and distinct materials prepared from iPPH. As aforementioned, an unvarying area in this temperature interval is seen for the pristine mesostructure. An evident discontinuity is, however, noted at around 100 °C in the composites.

Presence of polymeric chains within the channel nanospaces indicates that these materials are nanocomposites, although most polymeric chains are outside the mesoporous silica since its content in the ultimate materials is not really elevated. Moreover, the highest SBA-15 amount incorporated by extrusion in these materials under analysis seems to be near to the maximum one allowed to be added through this approach as deduced from closeness to rheological percolation achieved from viscoelastic characterization in the molten state.

On the other hand, Figure 9c compares variation in area of the (100) SBA-15 diffraction normalized to the initial value at room temperature for iPPSBA12L and iPPSBA13H. A clear displacement to higher temperature is observed for the discontinuity location in the iPPSBA12L composite. It appears at around 112 °C, which is 9 °C above that exhibited by iPPSBA13H. This shift

confirms the observation described from DSC results, where it was commented that materials prepared from iPPL showed the minor endothermic event at temperatures higher than that found in the composites obtained from iPPH. It seems, therefore, that thicker crystallites can be developed within SBA-15 channels when iPP M_w is reduced in these materials prepared by extrusion.

The effect of iPP molecular weight and of the amount of SBA-15 on the mechanical properties has been analyzed from stress-strain measurements. Figure 10 represents the Young´s modulus values attained in all of these materials. Two clear effects are seen. The first one is related to the pristine homopolymers. Thus, iPPL shows an elastic modulus higher than the neat iPPH. The second observation is the reinforcement role of the SBA-15 incorporation, which is enlarged as much as its content rises.

The higher rigidity shown by iPPL can be related to its smaller M_w. Firstly, the crystallinity is slightly higher than in the case of iPPH composites [71]. Important differences are also seen in Figure 1c and 1d between the values of viscosity exhibited by the two homopolymers, although their molecular weight does not differ very much. This fact indicates the weakness in intra e intermolecular interactions for the iPPL. Consequently, extent of entanglements is not very significant and its macrochains become stiffer and fragile, as deduced from the small values of elongation at break reported in Table 3.

A less important reduction in the elongation at break has been reported by introduction of some polar groups in the iPP architecture because of the improvement in the adhesion at interface [72]. Nevertheless, elastic modulus is much smaller in those samples due to the chain regularity interruptions introduced by those additional functionalities.

4. Conclusions

Various nanocomposites based on mesoporous SBA-15 silica and two different isotactic polypropylenes (iPP) have been prepared by melt extrusion in order to evaluate the influence of average molecular weight on different features. In the two cases, a rather uniform and random

distribution of SBA-15 particles is observed within the iPP matrix, without existence of inorganic domains of large size across the surface.

Molecular weight affects, however, the rheological behavior, the thermal stability, the crystallization process of the iPP chains (located either within the nanometric SBA-15 mesostructure or out of silica particles), and the mechanical response. Thus, although rheological magnitudes are primarily changed by the amount of SBA-15, their reinforcement effect in the molten iPP matrix seems to be more important at high contents as molecular weight decreases.

Moreover, incorporation of mesoporous SBA-15 increases thermal stability under the two environments analyzed. In inert atmosphere, maximum degradation temperature is moved to higher temperatures in the composites prepared from iPPH compared with those obtained from iPPL. Under oxidative conditions, hindrance of the air diffusion into the iPP bulk in presence of SBA-15 is, however, rather independent of molecular weight.

A clear dependence with iPP molecular weight has been also found for the endotherm ascribed to melting of the iPP crystallites confined inside the nanometric channels of the SBA-15 (appearing at temperatures significantly lower than the main melting process). Thus, the endotherm for the confined iPP crystals in the case of iPPL is located at temperatures noticeably higher than in the iPPH nanocomposites. This feature has been confirmed by real-time variable-temperature small-angle X-ray scattering (SAXS) measurements with synchrotron radiation, through the observation of a discontinuity in the variation with temperature of the area of the (100) SBA-15 diffraction. These results suggest thicker confined crystals in the composites prepared from iPPL.

Furthermore, chains of iPPL are able to initiate their crystallization at temperatures higher than those found in the iPPH based materials and lead to slightly higher degrees of crystallinity. These structural details promote a superior rigidity in iPPL and its nanocomposites.

Acknowledgements

This work was supported by the Agencia Estatal de Investigación (AEI, Spain) together with the European Regional Development Fund (FEDER, UE) (MAT2016-79869-C2-1-P). Ms. R Barranco-García also thanks her pre-doctoral funding (BES-2014-070972) associated with the MINECO (MAT2013-47972-C2-1-P) project. The synchrotron experiments were performed at beamline BL11-NCD at ALBA Synchrotron Light Facility with the collaboration of ALBA staff. Authors are grateful for the funding received to perform these measurements.

5. References

[1] D. B. Malpass, E. I. Band, "Introduction to polymers of propylene," in Introduction to Industrial polypropylene: Properties, Catalysis, Processes (Scrivener, 2012), pp. 1–18

[2] B. Pukanszky, J. Moczo, Macromol. Symp. 214 (2004) 115–134. https://doi.org/10.1002/masy.200451009.

[3] J.I. Weon, H.J. Sue, J. Mater. Sci. 41 (8) (2006) 2291–2300. https://doi.org/10.1007/s10853-006-7171-x.

[4] V. Hristov, M. Krumova, G. Michler, Macromol. Mater. Eng. 291 (2006) 677–683. https://doi.org/10.1002/mame.200500409.

[5] P. Rungruang, B.P. Grady, P. Supaphol, Coll. Surf. A-Phys Eng. Aspects. 275 (2006) 114–125. https://doi.org/10.1016/j.colsurfa.2005.09.029.

[6] M. Avella, S. Cosco, M.L. Di Lorenzo, M.E. Errico, G. Gentile, Macromol. Symp. 234 (2006) 156–162. https://doi.org/10.1002/masy.200650220.

[7] M.A. Santos, A.M. Maliska, A.N. Klein, W. Ristow, J.L.R. Muzart, Mater. Sci. Eng. Part A 407 (1–2) (2005) 71–76. https://doi.org/10.1016/j.msea.2005.06.026.

[8] J.Z. Liang, F.H. Li, Polym. Test. 26 (2007) 1025–1030. https://doi.org/10.1016/j.polymertesting.2007.07.002.

[9] A. Kubacka, M.L. Cerrada, C. Serrano, M. Fernández-García, M. Ferrer, M. Fernández-García, J. Nanosci. Nanotech. 8 (2008) 3241–3246. https://doi.org/10.1166/jnn.2008.363.

[10] M.L. Cerrada, C. Serrano, M. Sánchez-Chaves, M. Fernández-García, M.A. de Andrés, R.J. Riobóo, F. Fernández-Martín, A. Kubacka, M. Ferrer, M. Fernández-García, Environ. Sci. Techn. 43 (2009) 1630–1634. https://doi.org/10.1021/es801968r.

[11] E. Blázquez-Blázquez, J. Arranz-Andrés, J. Ressia, E.M. Vallés, P. Marín, A.M. Aragón, E. Pérez, M.L. Cerrada, Polym. Test. 72, 263–270 (2018). https://doi.org/10.1016/j.polymertesting.2018.10.031.

[12] L. Sangroniz, M.A. Moncerrate, V.A. De Amicis, J.K. Palacios, M. Fernández, A. Santamaría, J.J. Sánchez, F. Laoutid, P. Dubois, A.J. Muller, J. Polym. Sci., Part B-Polym. Phys. 53 (2015) 1567–1579. https://doi.org/10.1002/polb.23786.

[13] M. Ahsani, R. Yegani, Chem. Eng. Res. Design 102 (2015) 261–273. https://doi.org/ 10.1016/j.cherd.2015.06.035.

[14] F. Zoukrami, N. Haddaoui, M. Sclavons, J. Devaux, C. Vanzeveren, Polym. Bull. 75 (2018) 5551–5566. https://doi.org/10.1007/s00289-018-2344-8.

[15] G. Li, F. Wang, P. Liu, C. Gao, Y.F. Ding, S.M. Zhang, M.S. Yang, Appl. Surf. Sci. 476 (2019) 682–690. https://doi.org/10.1016/j.apsusc.2019.01.116.

[16] S.Y. Ding, P. Liu, C. Gao, F. Wang, Y.F. Ding, S.M. Zhang, M.S. Yang, Polym. Adv. Technol. 30 (2019) 1116–1125. https://doi.org/10.1002/pat.4545.

[17] J.S. Beck, J.C. Vartuli, W.J. Roth, M.E. Leonowicz, C.T. Kresge, K.D. Schmitt, C.T.-W. Chu, D.H. Olson, E.W. Sheppard, S.B. McCullen, J.B. Higgins, J.L. Schlenkert, J. Am. Chem. Soc. 114 (1992) 10834−10843. https://doi.org/10.1021/ja00053a020.

[18] D.Y. Zhao, J.L. Feng, Q.S. Huo, N Melosh, G.H. Fredrickson, B.F. Chmelka, G.D. Stucky, Science 279 (1998) 548−552. https://doi.org/10.1126/science.279.5350.548.

[19] W.J. Roth, J.C. Vartuli, Zeolites and Ordered Mesoporous Materials: Progress And Prospects Book Series: Studies in Surface Science and Catalysis, Volume: 157 (2005) 91–110.

[20] X.C. Dong, L, Wang, G.H. Jiang, Z.R. Zhao, T.X. Sun, H.J. Yu, W.Q. Wang, J. Mol. Catal. A−Chem. 240 (2005) 239−244. https://doi.org/10.1016/j.molcata.2005.06.060.

[21] G.C. Xu, A.Y. Li, L. De Zhang, X.Y. Yu, T. Xie, G.S. Wu, J. Reinforced Plastics and Composites, 23 (2004) 1365−1372. https://doi.org/10.1177/0731684404037044.

[22] J.M. Campos, M.R. Ribeiro, J.P. Lourenço, A. Fernandes, J. Mol. Catal. A−Chem. 277 (2007) 93–101. https://doi.org/10.1016/j.molcata.2007.07.026.

[23] J.M. Campos, J.P. Lourenço, H. Cramail, M.R. Ribeiro, Prog. Polym. Sci. 37 (2012) 1764−1804. https://doi.org/10.1016/j.progpolymsci.2012.02.006.

[24] S. Kim, E. Marand, Micropor. Mesopor. Mat. 114 (2008) 129–136. https://doi.org/10.1016/j.micromeso.2007.12.028.

[25] A. Jomekian, M. Pakizeh, A. R. Shafiee, S. A. A. Mansoori, Sep. Purif. Technol. 80 (2011) 556–565. https://doi.org/10.1016/j.seppur.2011.06.011.

[26] A. Jomekian, S. A. A. Mansoori, N. Monirimanesh, A. Shafiee, Korean J. Chem. Eng. 28 (2011) 2069-2075. https://doi.org/10.1007/s11814-011-0075-8.

[27] A. Bento, J.P. Lourenço, A. Fernandes, M.R. Ribeiro, J. Arranz-Andrés, V. Lorenzo, M.L. Cerrada, J. Membrane Sci. 415–416, 702-711 (2012). https://doi.org/10.1016/j.memsci.2012.05.058.

[28] M.L. Cerrada, E. Pérez, J.P. Lourenço, J.M. Campos, M.R. Ribeiro, Micropor. Mesopor. Mat. 130 (2010) 215−223. https://doi.org/10.1016/j.micromeso.2009.11.009.

[29] M.L. Cerrada, E. Pérez, J.P. Lourenço, A. Bento, M.R. Ribeiro, Polymer 54 (2013) 2611−2620. https://doi.org/ 10.1016/j.polymer.2013.03.010.

[30] M.L. Cerrada, A. Bento, E. Pérez, V. Lorenzo, J. P. Lourenço, M. R. Ribeiro, Micropor. Mesopor. Mat. 232 (2016) 86-96. https://doi.org/10.1016/j.micromeso.2016.06.011.

[31] A.E. Ferreira, M.L. Cerrada, E. Pérez, V. Lorenzo, H.Cramail, J.P. Lourenço, M.R. Ribeiro, Micropor. Mesopor. Mat. 232 (2016) 13-25. https://doi.org/10.1016/j.micromeso.2016.06.002.

[32] A.E. Ferreira, M.L. Cerrada, E. Pérez, V. Lorenzo, H.Cramail, J.P. Lourenço, R.Quijada, M.R. Ribeiro. Eur. Polym. J. 85 (2016) 298–312. https://doi.org/10.1016/j.eurpolymj.2016.10.033.

[33] A.E. Ferreira, M.L. Cerrada, E. Pérez V. Lorenzo, E. Vallés, J. Ressia, H. Cramail, J.P. Lourenço, M.R. Ribeiro. eXPRESS Polymer Letters 11 (2017) 344–361. https://doi.org/10.3144/ expresspolymlett.2017.34.

[34] R. Barranco-García, A.E. Ferreira, M.R. Ribeiro, V. Lorenzo, A. García-Peñas, J.M. Gómez-Elvira, E. Pérez, M.L. Cerrada, Polymer 151 (2018) 218–230. https://doi.or g/10.1016/j.polymer.2018. 07.072.

[35] R. Barranco-García, J.M. López-Majada, J.C. Martínez, J.M. Gómez-Elvira, E. Pérez, M.L. Cerrada, Micropor. Mesopor. Mat. 272 (2018) 209–216. https://doi.org/10.1016/j.micromeso.2018. 06.032.

[36] A. Deryło-Marczewska, M. Zienkiewicz-Strzałka, K. Skrzypczyńska, Andrzej Światkowski, Krzysztof Kuśmierek, Adsorption 22 (2016) 801–812. https://doi.org/10.1007/s10450-016-9779-8.

[37] J. Brandrup, E.H. Imergut, E.A. Grulke, Eds., Polymer Handbook, 4th ed.; John Wiley and Sons, New York, 1999.

[38] J.D. Ferry, Viscoelastic Properties of Polymers, 3rd ed., John Wiley and Sons, New York, 1980.

[39] E.B. Bond, J.E. Spruiell, J.S. Lin, J. Polym. Sci., Part B-Polym. Phys. 37 (1999) 3050−3064. https://doi.org/ 10.1002/(SICI)1099-0488(19991101)37:21<3050::AID-POLB14>3.0.CO;2-L.

[40] R. Krache, R. Benavente, J.M. López-Majada, J.M. Pereña, M.L. Cerrada, E. Pérez, Macromolecules 40 (2007) 6871−6878. https://doi.org/10.1021/ma0710636.

[41] E. Pérez, M.L. Cerrada, R. Benavente, J.M. Gómez-Elvira, Macromol. Res. 19 (2011) 1179−1185. https://doi.org/10.1007/s13233-011-1103-6.

[42] J.L. de la Fuente, M. Wilhelm, H.W. Spiess, E.L. Madruga, M. Fernández Garcia, M.L. Cerrada, Polymer 46 (2005) 4544−4553. https://doi.org/ 10.1016/j.polymer.2005.03.076.

[43] Q. Zhang, L.A. Archer, Langmuir 18 (2002) 10435–10442. https://doi.org/10.1021/la026338j.

[44] Y. Song, Q. Zheng, Prog. Mater. Sci. 84 (2016) 1-58. https://doi.org/ 10.1016/j.pmatsci.2016.09.002.

[45] W. Bahloul, V. Bounor-Legaré, L. David, P. Cassagnau, J. Polym. Sci., Part B-Polym. Phys. 48 (2010) 1213–1222. https://doi.org/ 10.1002/polb.22012.

[46] C. Serrano, M.L. Cerrada, M. Fernández-García, J. Ressia, E.M. Vallés, Eur. Polym. J. 48 (2012) 586–596. https://doi.org/10.1016/j.eurpolymj.2011.12.012.

[47] J. Aguado, D.P. Serrano, M.D. Romero, J.M. Escola, Chem. Commun. 6 (1996), 725–726. 10.1039/cc9960000725.

[48] A. Marcilla, A. Gómez-Siurana, S. Menargues, R. Ruiz-Femenia, J. C. García-Quesada, J. Anal. Appl. Pyrolysis 76 (2006), 138–143. https://doi.org/ 10.1016/j.jaap.2005.10.004.

[49] J.M. Campos, J.P. Lourenço, E. Pérez, M.L. Cerrada, M. R. Ribeiro, J. Nanosci. Nanotech. 9 (2009) 3966–3974. https://doi.org/10.1166/jnn.2009.1298.

[50] H.-W. Wong, L.J. Broadbelt, Ind. Eng. Chem. Res. 40 (2001) 4716−4723. https://doi.org/ 10.1021/ie010171s.

[51] L. Achimsky, L. Audouin, J. Verdu, J. Rychly, L. Matisova-Rychla, Polym. Degrad. Stab. 58 (1997) 283−289. https://doi.org/10.1016/S0141-3910(97)00059-1.

[52] H. Nakatani, S. Suzuki, T. Tanaka, M. Terano, Polymer 46 (2005) 12366−12371. https://doi.org/ 10.1016/j.polymer.2005.10.131.

[53] R. Barranco-García, M.L. Cerrada, J.A. Ressia, E.M. Vallés, A. García-Peñas, E. Pérez, J.M. Gómez-Elvira, Polymer Degradation and Stability 154 (2018) 211-221. https://doi.org/ 10.1016/ j.polymdegradstab.2018.06.006.

[54] C.L. Jackson, G.B. McKenna. The melting behavior of organic materials confined in porous solids. J. Chem. Phys. 93, 9002 (1990). https://doi.org/10.1063/1.459240.

[55] G. Natta; P. Corradini, Nuovo Cimento Suppl. 15 (1960) 40−51. https://doi.org/ 10.1007/BF02731859.

[56] A.T. Jones, J.M. Aizlewood, D.R. Beckett, Makromol. Chem. 75 (1964) 134−158.

[57] S. Brückner, S.V. Meille, V. Petraccone, B. Pirozzi, Prog. Polym. Sci. 16 (1991) 361−404. https://doi.org/10.1016/0079-6700(91)90023-E.

[58] J.J. Varga, J. Macromol. Sci.– Phys. B 41 (2002) 1121−1171. https://doi.org/10.1081/MB-120013089.

[59] I.L. Hosier, R.G. Alamo, P. Esteso, J.R. Isasi, L. Mandelkern, Macromolecules 36 (2003) 5623−5636. https://doi.org/10.1021/ma030157m.

[60] B. Poon, M. Rogunova, A. Hiltner, E. Baer, S.P. Chum, A. Galeski. E, Piorkowska, Macromolecules 38 (2005) 1232−1243. https://doi.org/10.1021/ma048813l.

[61] C. De Rosa, S. Dello Iacono, F. Auriemma, E. Ciaccia, L. Resconi, Macromolecules 39 (2006) 6098−6109. https://doi.org/10.1021/ma0606354.

[62] C. De Rosa, O.R. Ballesteros, F. Auriemma, M.R. Di Caprio, Macromolecules 45 (2012) 2749−2763. https://doi.org/ 10.1021/ma201849w.

[63] E. Pérez, J.M. Gómez-Elvira, R. Benavente, M.L. Cerrada, Macromolecules 45 (2012) 6481–6490. https://doi.org/10.1021/ma3012834.

[64] J. Arranz-Andrés, R. Parrilla, M.L. Cerrada, E. Pérez. Macromolecules 46 (2013) 8557−8568. https://doi.org/10.1021/ma401539u.

[65] L. Boragno, P. Stagnaro, F. Forlini, F. Azzurri, G.C. Alfonso, Polymer 54 (2013) 1656−1662. https://doi.org/10.1016/j.polymer.2013.01.041.

[66] A. García-Peñas, J.M. Gómez-Elvira, R. Barranco-García, E. Pérez, M.L. Cerrada, Polymer 99 (2016) 112−121. https://doi.org/10.1016/j.polymer.2016.07.009.

[67] A. García-Peñas, J.M. Gómez-Elvira, V. Lorenzo, E. Pérez, M.L. Cerrada, Polymer 130 (2017) 17−25. https://doi.org/10.1016/j.polymer.2017.10.006.

[68] H. Palza, J.M. López-Majada, R. Quijada, J.M. Pereña, R. Benavente, E. Pérez, M.L. Cerrada, Macromol. Chem. Phys. 209 (2008) 2259–2267. https://doi.org/10.1002/macp.200800294.

[69] X. Wang, X. Ma, Ch. Song, D.R. Locke, S. Siefert, R.E. Winans, J. Möllmer, M. Lange, A. Möller, R. Gläser, Micropor. Mesopor. Mater. 169 (2013) 103–111. https://doi.org/ 10.1016/j.micromeso.2012. 09.023.

[70] R. Barranco-García, J.M. López-Majada, V. Lorenzo, J.M. Gómez-Elvira, E. Pérez, M.L. Cerrada, J. Membrane Sci. 569, 137-148 (2019). https://doi.org/10.1016/j.memsci.2018.10.009.

[71] Fonseca, J. M. Pereña, R. Benavente, M. L. Cerrada, A. Bello, E. Pérez, Polymer 36, 1887-1892, (1995). https://doi.org/10.1016/0032-3861(95)90936-V.

[72] R. Watanabe, H. Hagihara, H. Sato. Polym. J. 50 (2018) 1057–1065. https://doi.org/ 10.1038/ s41428-018-0095-x.

Table 1. Values of storage and loss moduli at 100 and 0.1 rad/s and at 200 °C for the iPP homopolymers and the different composites under study.

Composites based on iPP of low M_w					Composites based on iPP of high M_w				
sample	G′ (Pa)	G″ (Pa)	G′ (Pa)	G″ (Pa)	sample	G′ (Pa)	G″ (Pa)	G′ (Pa)	G″ (Pa)
	100 rad/s		0.1 rad/s			100 rad/s		0.1 rad/s	
iPPL	4840	12600	0.03	21	iPPH	21520	31150	0.85	87
iPPSBA2L	5935	13190	0.03	21	iPPSBA1H	18500	26790	0.65	77
iPPSBA4L	6065	13400	0.03	22	iPPSBA4H	21880	28520	0.90	88
iPPSBA7L	6490	13430	0.08	24	iPPSBA8H	24940	32830	2.90	105
iPPSBA12L	22480	31410	375	425	iPPSBA13H	77490	77490	265	805

Table 2. SBA-15 wt.% content calculated from TGA measurements under nitrogen and oxidative conditions, and average between them; melting (T_m) and crystallization temperatures (T_c), and overall crystallinity (normalized to the actual iPP content in the material) estimated by WAXD (f_c^{WAXD}) and DSC (f_c^{DSC}).

Sample	SBA-15^{inert} wt.%	SBA-15$^{oxid.}$ wt.%	average SBA-15 wt.%	f_c WAXD	T_m (°C)	f_c^{DSC}	T_C (°C)
iPPL	0	0	0	0.63	143.0	0.63	117.5
iPPSBA2L	1.5	2.6	2.1	0.63	142.5	0.64	110.5
iPPSBA4L	3.8	3.9	3.9	0.63	142.0	0.62	111.0
iPPSBA7L	6.9	7.4	7.2	0.62	142.0	0.63	111.5
iPPSBA12L	12.0	12.5	12.3	0.60	142.5	0.62	112.0
iPPH	0	0	0	0.60	142.0	0.60	114.0
iPPSBA1H	1.4	1.4	1.4	0.60	143.0	0.59	111.0
iPPSBA4H	3.9	3.9	3.9	0.59	143.0	0.61	111.0
iPPSBA8H	7.7	7.7	7.7	0.59	142.5	0.58	110.5
iPPSBA13H	12.9	12.7	12.8	0.58	142.5	0.61	110.0

Table 3. Mechanical parameters derived from stress–strain tests at 25 °C for the materials: average Young's modulus (E); yield stress (σ_Y); yield deformation (ε_Y); deformation at break (ε_{break}). SBA-15 wt.% content has been also listed.

sample	SBA-15 *wt.%* by TGA	E (MPa)	σ_Y (MPa)	ε_Y (%)	ε_{break} (%)
iPPL	0	1570	32.5	5.0	400
iPPSBA2L	1.5	1615	28.5	5.0	300
iPPSBA4L	3.8	1640	29.0	4.0	8
iPPSBA7L	6.9	1695	31.0	3.5	4
iPPSBA12L	12.0	1800	—[a]	—[a]	2.5
iPPH	0	1045	28.0	8.5	730
iPPSBA1H	1.4	1060	28.0	8.5	750
iPPSBA4H	3.9	1080	28.0	7.0	80
iPPSBA8H	8.0	1130	28.0	6.7	30
iPPSBA13H	12.8	1250	28.0	5.3	25

[a]Yielding point has not been reached at this composition for the different dumbbell-shaped strips.

Captions of Figures:

Figure 1. Frequency dependence curves at 200 °C of: a) and b): storage modulus, G´(ω); c) and d): viscosity, for iPP–SBA-15 composites at different SBA-15 contents with iPP of low (left) and high (right) molecular weight.

Figure 2. Frequency dependence curves at 200 °C of phase angle δ for iPP–SBA-15 composites at different SBA-15 contents with iPP of low (left) and high (right) molecular weight.

Figure 3. TGA curves under inert and oxidative atmospheres (top and bottom representations, respectively) for the materials prepared from iPP with low (left) and high (right) molecular weight and the different contents in SBA-15. Amplified insets in the middle show comparisons between several samples prepared from both iPPs.

Figure 4. Derivatives of TGA curves under inert (a) and oxidative atmospheres (b). Variation of temperatures of the maxima with the SBA-15 content for all the materials (c).

Figure 5. SEM micrographs for different materials (magnification 10,000x and scale bar 2 μm). On the top: iPPSBA7L (left) and iPPSBA12L (right); and, on the bottom: iPPSBA8H (left) and iPPSBA13H (right).

Figure 6. a) and b) DSC endotherms corresponding to the first melting run, shifted along Y axis for a better visualization, for samples prepared from iPP with low and high M_w, respectively; c) and d) DSC exotherms attained during crystallization process for the materials prepared from iPP with low and high M_w, respectively.

Figure 7. Synchrotron WAXD 1D diffractograms at room temperature for the different materials extruded from: a) iPPL and b) iPPH at the different SBA-15 contents analyzed.

Figure 8. SAXS profiles achieved during the first melting process for SBA-15 (left) and for the iPPSBA1H nanocomposite (right). Only one of every two frames is plotted for clarity.

Figure 9. a) SAXS profiles during the first melting process for the different nanocomposites prepared from iPPL at the *s* interval corresponding to the first order of SBA-15 hexagonal arrangement. Curves were shifted for a better understanding; b) temperature dependence of area for the main SBA-15 SAXS peak in the neat SBA-15 and different nanocomposites (iPPSBA13H, iPPSBA8H and iPPSBA4H) extruded from iPPH during first melting experiments. Results were normalized to a relative area of 100 for pure SBA-15 powder; c) temperature variation of area for the main SBA-15 SAXS peak, normalized to its value at 20 °C, for iPPSBA12L and iPPSBA13H during melting experiments.

Figure 10. Values of modulus determined from stress-strain measurements for the two iPP homopolymers and their nanocomposites with different SBA-15 contents.

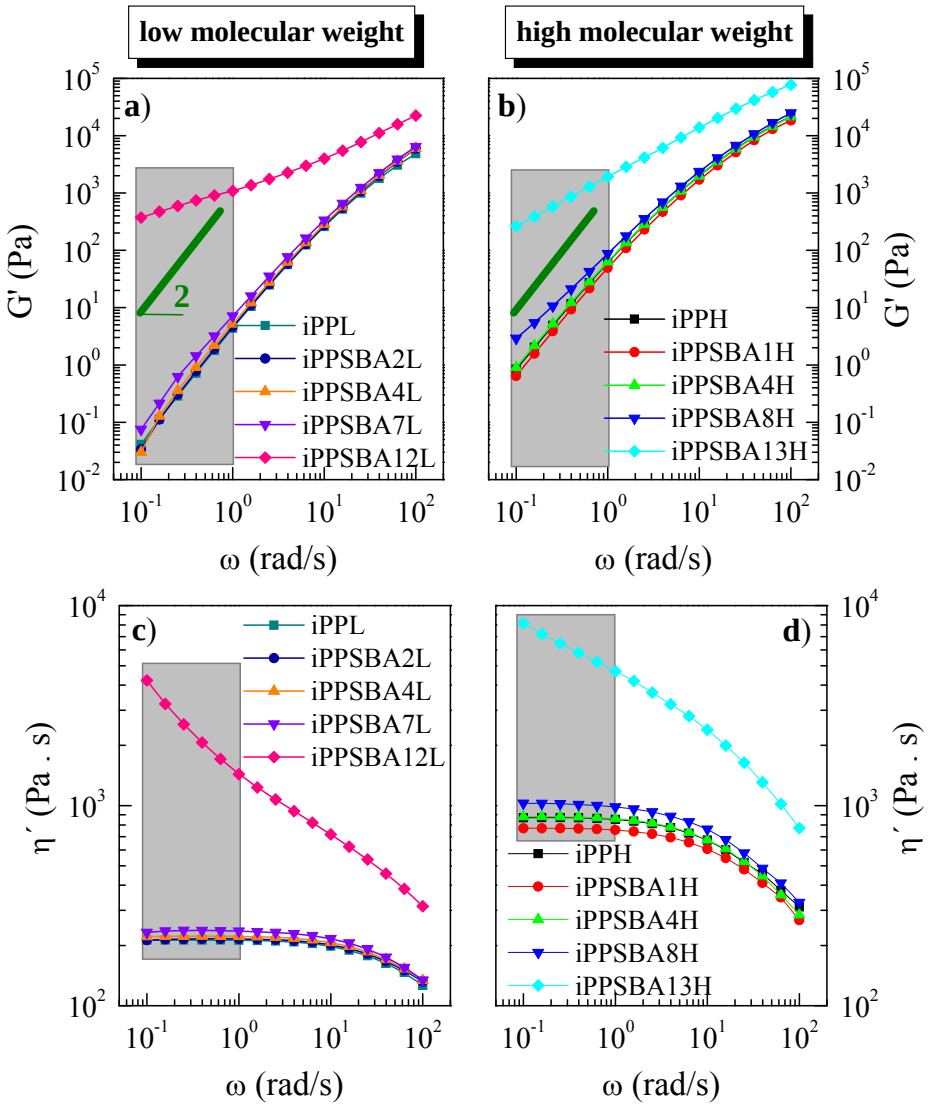

Figure 1

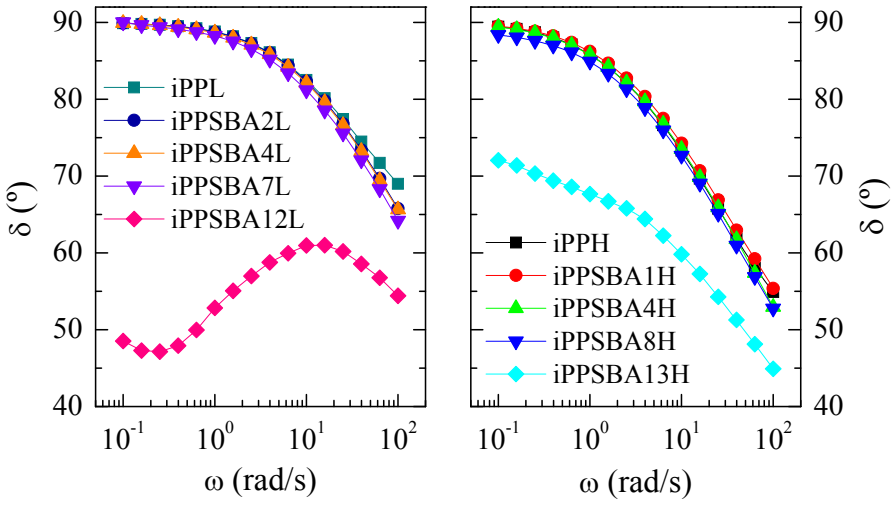

Figure 2

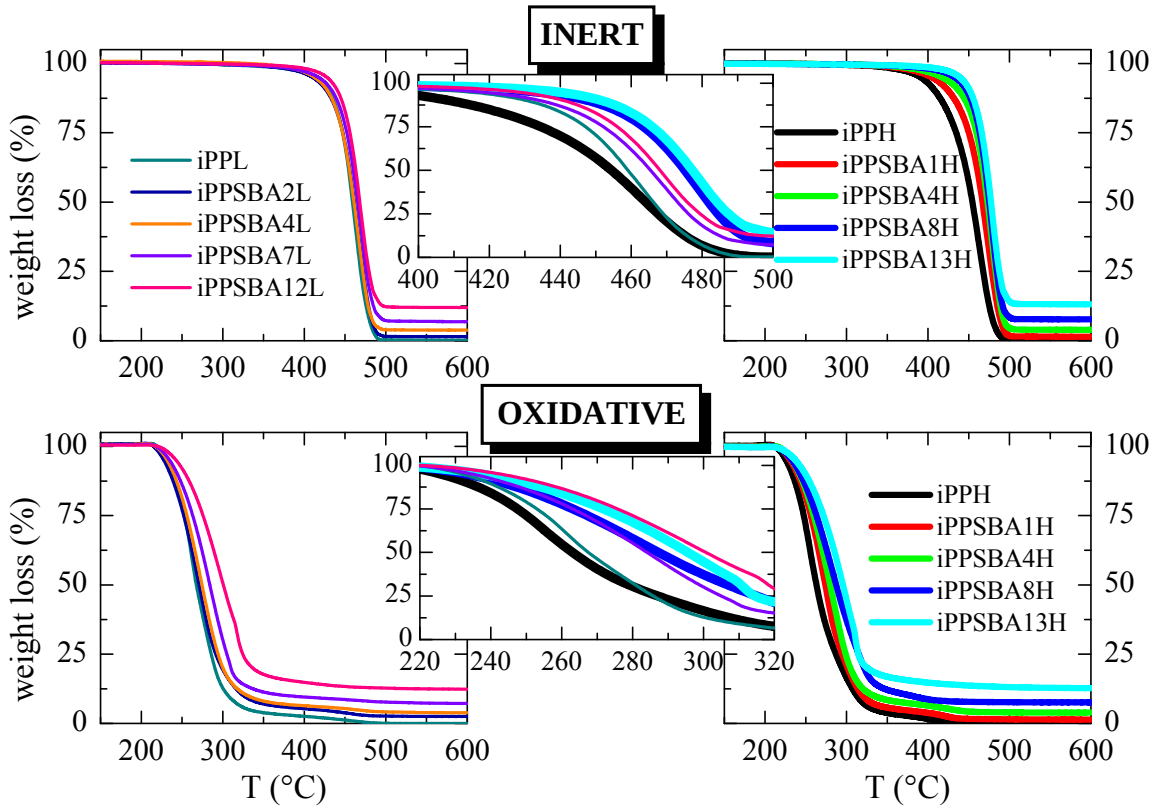
INERT
OXIDATIVE
weight loss (%)
T (°C)
iPPL
iPPSBA2L
iPPSBA4L
iPPSBA7L
iPPSBA12L
iPPH
iPPSBA1H
iPPSBA4H
iPPSBA8H
iPPSBA13H

Figure 3

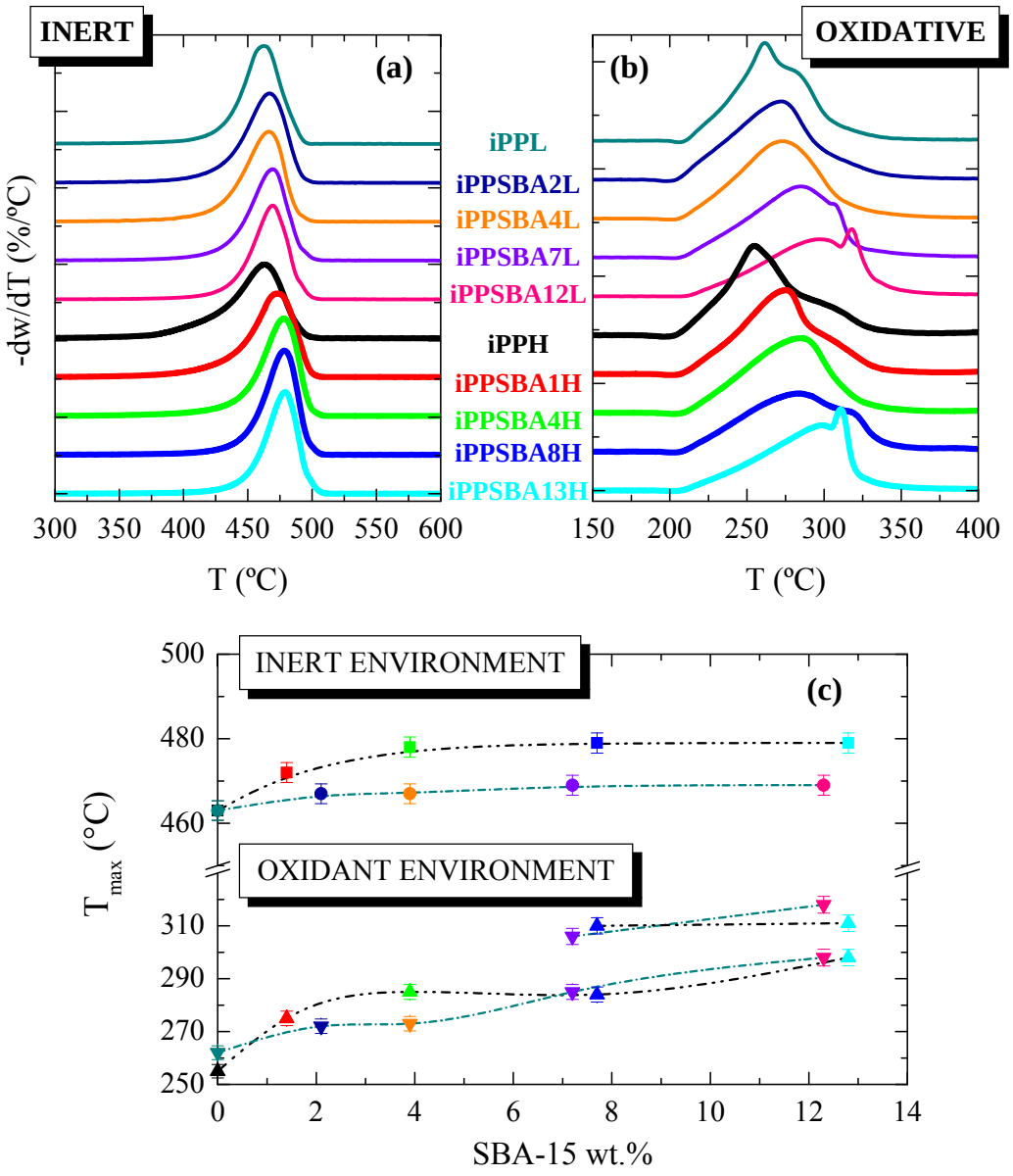
INERT
(a)
OXIDATIVE
(b)
-dw/dT (%/ºC)
iPPL
iPPSBA2L
iPPSBA4L
iPPSBA7L
iPPSBA12L
iPPH
iPPSBA1H
iPPSBA4H
iPPSBA8H
iPPSBA13H
300 350 400 450 500 550 600
T (ºC)
150 200 250 300 350 400
T (ºC)
INERT ENVIRONMENT
(c)
OXIDANT ENVIRONMENT
T max (°C)
500
480
460
310
290
270
250
0 2 4 6 8 10 12 14
SBA-15 wt.%

Figure 4

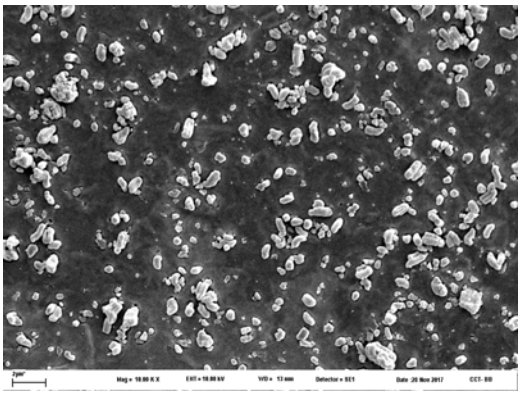

iPPSBA7L

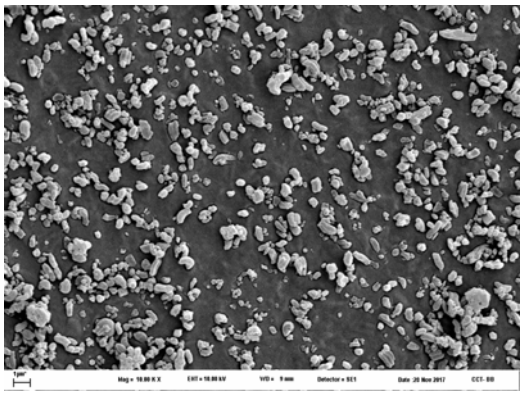

iPPSBA12L

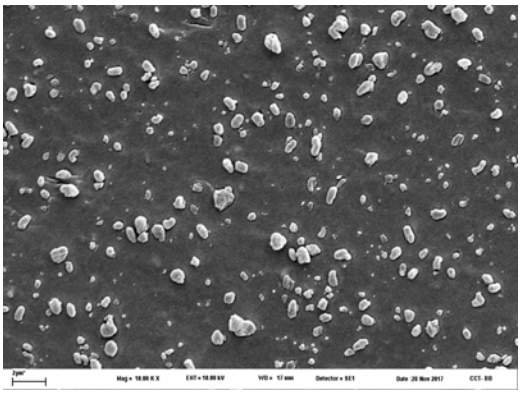

iPPSBA8H

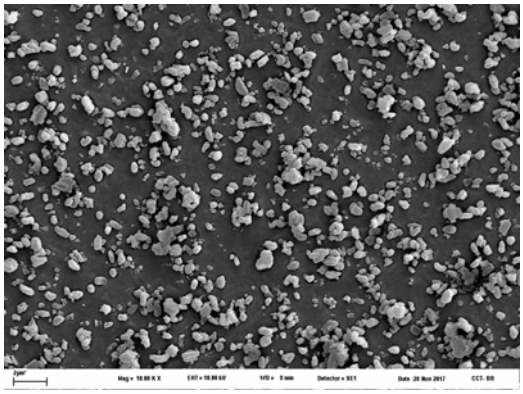

iPPSBA13H

Figure 5

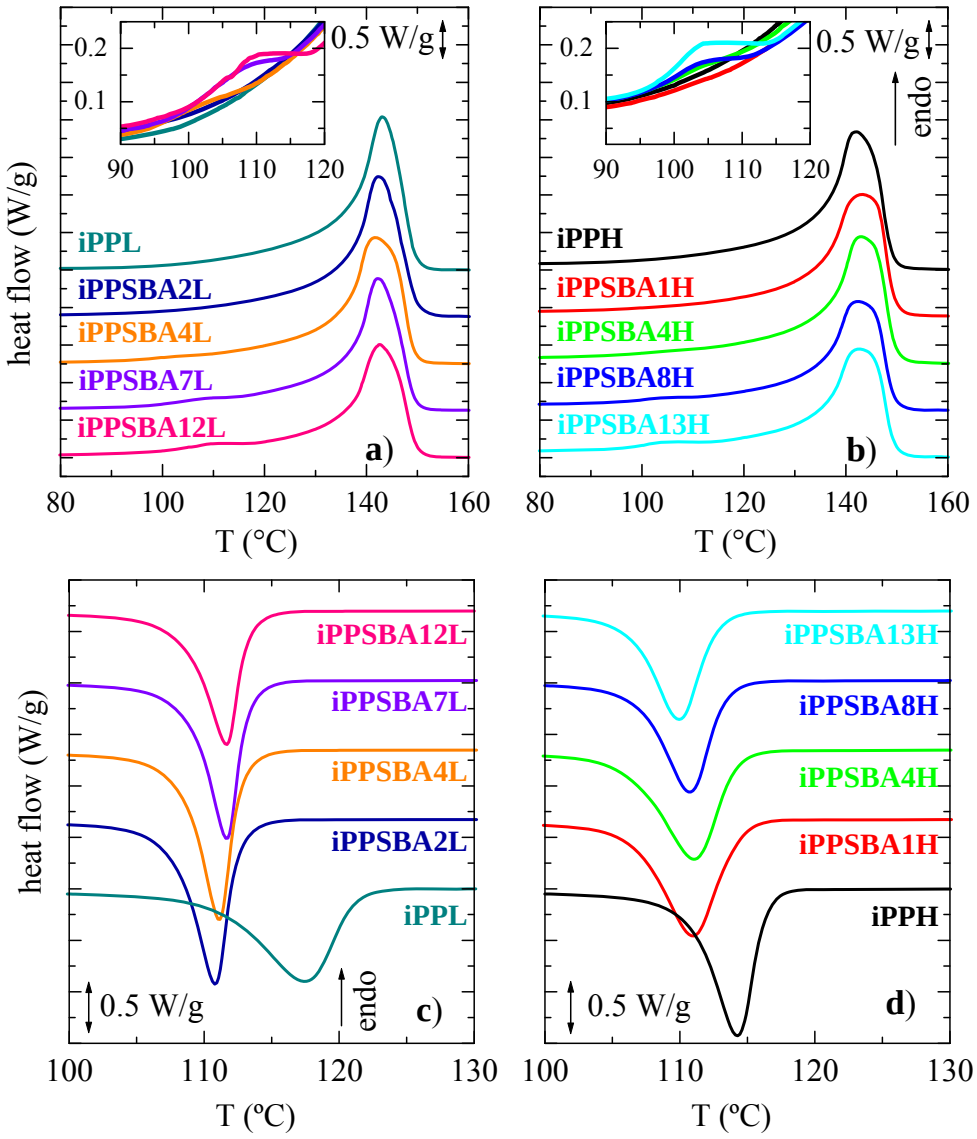
heat flow (W/g)
0.5 W/g
0.2
0.1
90 100 110 120
iPPL
iPPSBA2L
iPPSBA4L
iPPSBA7L
iPPSBA12L
a)
80 100 120 140 160
T (°C)
iPPH
iPPSBA1H
iPPSBA4H
iPPSBA8H
iPPSBA13H
endo
b)
iPPSBA12L
iPPSBA7L
iPPSBA4L
iPPSBA2L
iPPL
c)
100 110 120 130
T (°C)
iPPSBA13H
iPPSBA8H
iPPSBA4H
iPPSBA1H
iPPH
d)

Figure 6

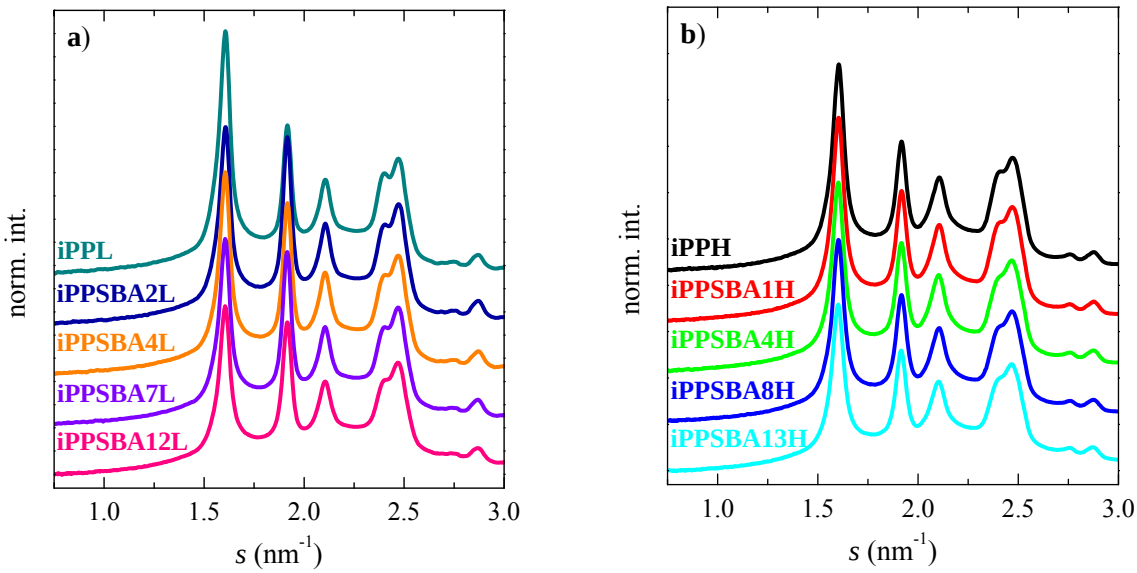

Figure 7

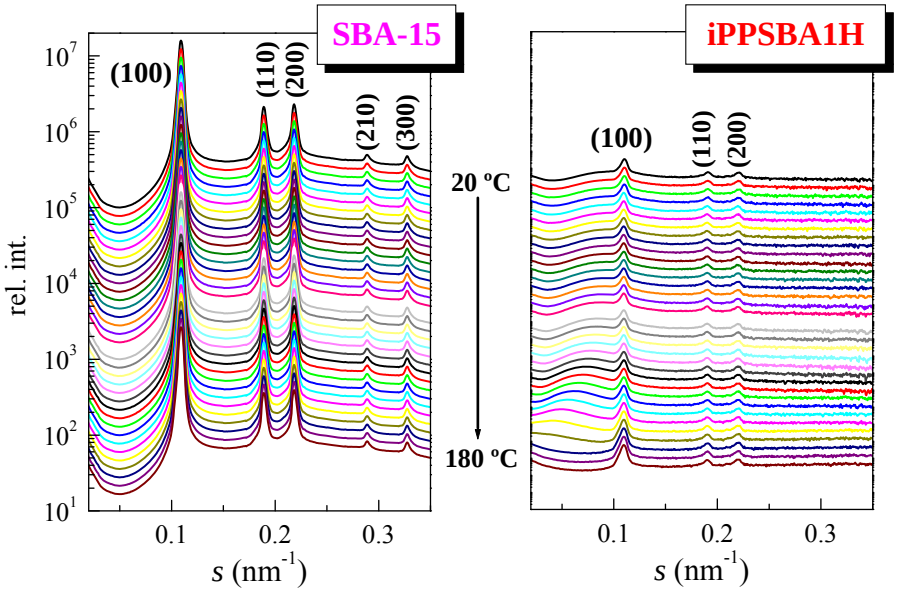

Figure 8

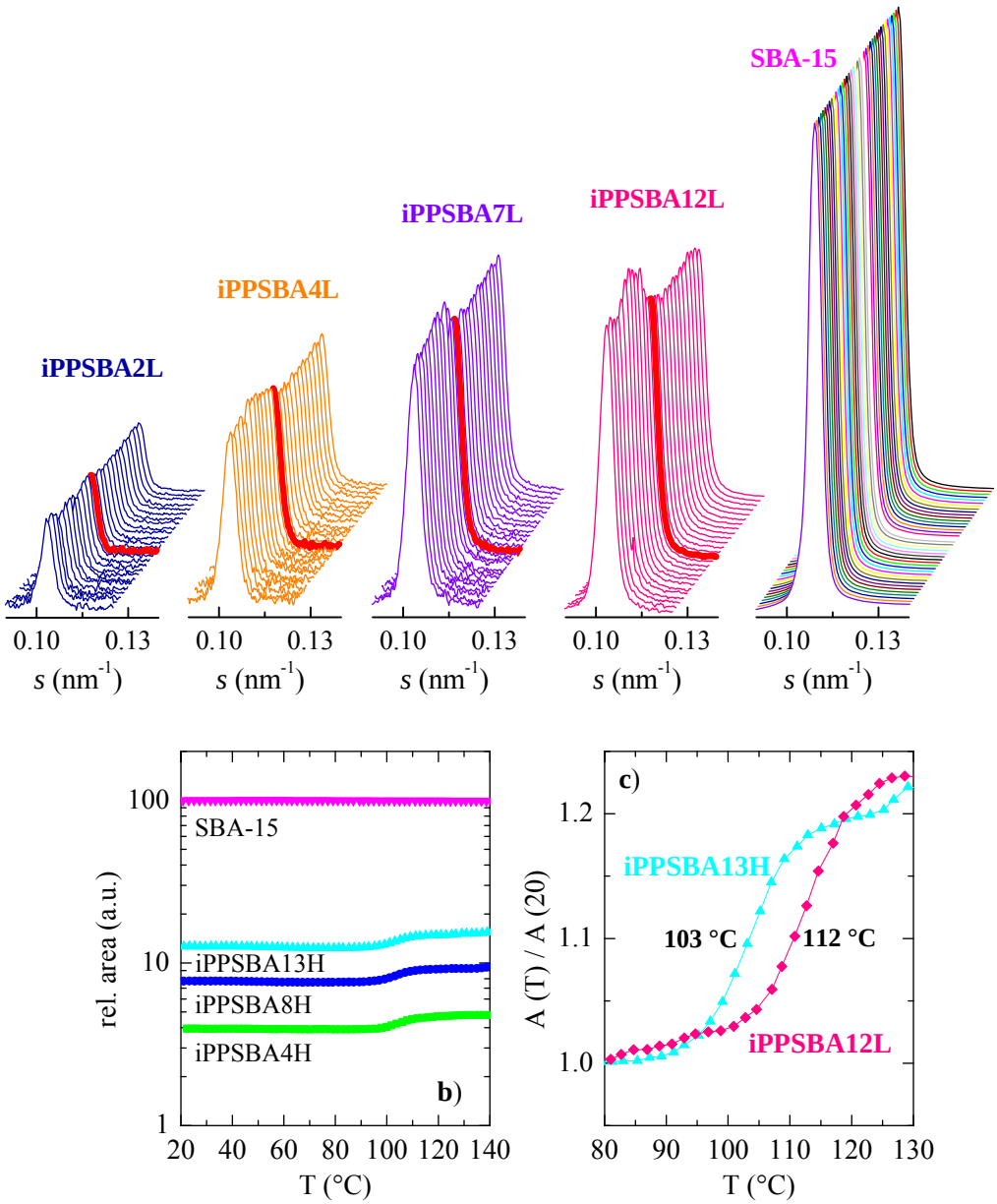
SBA-15
iPPSBA12L
iPPSBA7L
iPPSBA4L
iPPSBA2L
0.10
0.13
s (nm-1)
100
10
1
rel. area (a.u.)
SBA-15
iPPSBA13H
iPPSBA8H
iPPSBA4H
b)
20 40 60 80 100 120 140
T (°C)
c)
1.2
1.1
1.0
A (T) / A (20)
iPPSBA13H
103 °C
112 °C
iPPSBA12L
80 90 100 110 120 130
T (°C)

Figure 9

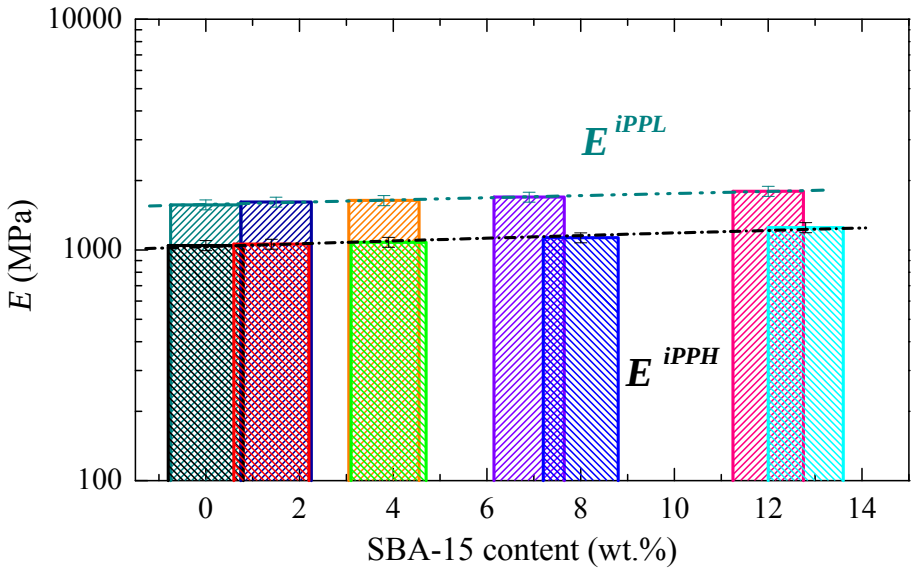
10000
1000
100
E (MPa)
E iPPL
E iPPH
0
2
4
6
8
10
12
14
SBA-15 content (wt.%)

Figure 10